Published in final edited form as:
ACS Nano. 2011 September 27; 5(9): 6945–6954. doi:10.1021/nn2014003.

Dispersions of Aramid Nanofibers: A New Nanoscale Building Block

Ming Yang[1], **Keqin Cao**[2], **Lang Sui**[3], **Ying Qi**[3], **Jian Zhu**[1], **Anthony Waas**[2,5], **Ellen M. Arruda**[2,4,6], **John Kieffer**[3], **M. D. Thouless**[2,3], and **Nicholas A. Kotov**[1,3,4]

[1]Department of Chemical Engineering, University of Michigan, Ann Arbor, MI, 48109-2136

[2]Department of Mechanical Engineering, University of Michigan, Ann Arbor, MI, 48109-2136

[3]Department of Materials Science and Engineering, University of Michigan, Ann Arbor, MI, 48109-2136

[4]Department of Biomedical Engineering, University of Michigan, Ann Arbor, MI, 48109-2136

[5]Department of Aerospace Engineering, University of Michigan, Ann Arbor, MI, 48109-2136

[6]Department of Macromolecular Science and Engineering, University of Michigan, Ann Arbor, MI, 48109-2136

Abstract

Stable dispersions of nanofibers are virtually unknown for synthetic polymers. They can complement analogous dispersions of inorganic components, such as nanoparticles, nanowires, nanosheets, *etc* as a fundamental component of a toolset for design of nanostructures and metamaterials *via* numerous solvent-based processing methods. As such, strong flexible polymeric nanofibers are very desirable for the effective utilization within composites of nanoscale inorganic components such as nanowires, carbon nanotubes, graphene, and others. Here stable dispersions of uniform high-aspect-ratio aramid nanofibers (ANFs) with diameters between 3 and 30 nm and up to 10 μm in length were successfully obtained. Unlike the traditional approaches based on polymerization of monomers, they are made by controlled dissolution of standard macroscale form of the aramid polymer, *i.e.* well known Kevlar threads, and revealed distinct morphological features similar to carbon nanotubes. ANFs are successfully processed into films using layer-by-layer (LBL) assembly as one of the potential methods of preparation of composites from ANFs. The resultant films are transparent and highly temperature resilient. They also display enhanced mechanical characteristics making ANF films highly desirable as protective coatings, ultrastrong membranes, as well as building blocks of other high performance materials in place of or in combination with carbon nanotubes.

Keywords

nanofibers; transparent nanocomposites; layer-by-layer assembly; LBL; Kevlar; aramid fibers

The structure of nanofibers from polymers is expected to bring about unique mechanical, electrical and optical properties, which are different from bulk materials similarly to the nanoscale versions of many metals or semiconductors. Polymer nanofibers should be considered as essential “building blocks” of the nanoscale toolset along with a large variety

Supporting Information *Available:* Details of backscattering setup for Brillouin scattering, typical results from nanoindentation experiments for PDDA/ANF_{300} LBL film with maximum depth set at 400 nm and the assignment of Kevlar active modes in Raman scattering. This material is available free of charge *via* the Internet at http://pubs.acs.org.

of inorganic “building blocks” well known in materials science, which include nanoparticles, nanowires, carbon nanotubes (CNTs), graphene, and clay nanosheets. Liquid dispersions of polymer nanofibrils analogous to those obtained for all the other inorganic nanoscale components (INCs) would be most useful for the functional design of nanocomposites and metamaterials. Variable permutations of organic components in the forms of molecular solutions or nanofiber dispersions and INCs will make possible property sets which are currently considered to be difficult or impossible to obtain.[1,2] However, the choice of polymer nanofiber dispersions is limited at best or not known for most polymers. Compared to dispersions of INCs this is virtually a virgin territory for both chemical and materials research.

Polymeric nanofibers are typically produced by electrospinning,[3] drawing,[4] template synthesis,[5] phase separation,[6] and self-assembly.[7] Electrospinning is probably the most widely used method for generating polymeric nanofibers with controlled diameters (from several nanometers to micrometers). This method is very useful for generation of solid nanofiber mats from many different polymers with typical diameters from tens of nanometers to tens of micrometers, but not for very small fibres comparable with CNT diameters or nanofiber dispersions. One can also obtain polymeric nanofibers by template synthesis, for instance in solid oxide matrices followed by their dissolution.[8,9] This approach can be modified for the preparation of multisegmented polymer--metal nanorods of interest for electronic devices,[10,11] but it is limited by only a few available templates, relatively large diameters exceeding 50 nm, and is restricted to the interfacial localization of the nanofibers. The yield of the nanorods made from templates is also very small.

The small amounts of material that can be produced and the inability to disperse nanofibers in liquid media are also characteristic for many nanofibers made by interfacial reactions. Many examples can be seen for electropolymerized nanofibers of conducting polymers, such as polyaniline nanowires, which typically produce fibrils with diameters of 50-70 nm.[12] There are also techniques for making polymeric nanofibers by phase separation,[6] or interfacial polymerization.[13,14] They can be convenient for preparation of solid porous materials, but are difficult to use as a general source of nanoscale organic components for materials design. The nanofibers made in this way often exceed 30 nm in diameter. An interesting technique that avoids the interfacial restrictions typical for the methods discussed above is the method of self-assembly of purposely designed organic surfactants.[7] This method can be compared to the assembly of inorganic nanoparticles,[15] and leads to smaller fibers with diameters of less than 10 nm. Some of the self-assembled organic fibers can be made in a dispersed state instead of the more common gels.[16] Although the synthesis of the corresponding surfactants requiring a combination of hydrophilic and hydrophobic blocks is quite complex, these nanofibers are quite interesting for biomedical applications as cell-growth matrices.[17] At the same time, they represent a substantial departure from the idea of polymeric nanofibers with predominantly axial orientation of molecular strands as obtained, for instance, by electrospinning. The radial orientation of the amphiphilic units and small area of interactions between them are not necessarily optimal for mechanical, electrical, and optical properties.

A unique case for dispersions of polymeric nanofibers is represented by cellulose.[18] A high activity in this area, a large variety of surface modifications, and a lot of interesting materials made from them[19-22] provide a great example of what might be possible for other polymeric nanofibers, especially for those with much better control of molecular structure. Acid hydrolysis is typically used for the production of cellulose nanofibers. Negative surface charge makes them easily dispersable in aqueous solvents.[23] Cellulose nanofibers are available in diameters between 3 and 30 nm depending on the particular source (such as wood pulp)[24] of the macroscale version of the material and on the subsequent series of

treatments.[24,25] Despite the large variety of potential sources of cellulose, the resultant nanofibers may not be ideal choices for many different applications. Their typical low aspect ratios and molecular rigidity compared with CNTs could diminish the advantage of nanofibers for effective stress-transfer in composites and the inherent hydrophilicity could result in the weak interactions with hydrophobic matrix materials.[26] When combined with INCs, their stiff molecular structures originating in packing of cyclic blocks of sugars revealed a problem[27] and therefore, the structural control and tunability of intermolecular interactions that comes with synthetic polymers is important.

One can see that there are no known examples of dispersions of synthetic polymer nanofibers in size matching those of CNTs, nanowires, nanoparticles and other INCs. There are three principal reasons we believe that finding methods for their preparation and utilization of a broader nanotechnology toolbox would be essential for further development of nanomaterials.

1. The progress in the broad area of high-performance mechanical properties is hampered by the availability of new high-strength flexible polymeric components. As an example, such nanofibers could be combined with other polymers with different functionalities to obtain coatings of polymer blends optimized for multiple performance characteristics. The size of the polymer fibrils is highly significant for a variety of properties and particularly for optical transparency.
2. Nanofiber dispersions could also be combined with INCs. To date, the mismatch between the mechanical properties of INCs and polymers, limited choice of flexible polymer fibers, the difficulty of dispersing INCs in a polymer matrix, and the lack of suitable chemically active groups for functionalizing the interfaces have inhibited widespread exploitation of excellent mechanical properties of INCs.
3. Availability of polymeric nanofiber dispersions opens new possibilities for processing of traditional materials, and therefore, properties that could be difficult or impossible to obtain with other forms of polymers.

These practical reasons as well as the academic novelty of polymeric nanofiber dispersions in general, and the research challenge of making polymeric structures with controlled association with each other prompted us to look for new synthetic approaches to such polymeric materials. As such, in this paper we demonstrate that careful dissociation of a macroscale version of Kevlar leads to the nanofiber form of this polymer. Indefinitely stable dispersions of uniform high-aspect-ratio aramid nanofibers (ANFs) with diameters between 3 and 30 nm controlled by the media composition and up to 10 μm in length were successfully obtained. Their morphologies reveal some similarities with carbon nanotubes and further research is likely to reveal more of such similarities. ANFs can also be processed in transparent thin films using layer-by-layer assembly (LBL) with superior mechanical performance.

Results and Discussion

Kevlar is a well-known ultra-strong para-aramid synthetic macroscale fiber with a high tensile strength-to-weight ratio.[28,29] Typical threads and fibers of Kevlar consist of long molecular chains produced from PPTA (poly-paraphenylene terephthalamide) between which there are inter-chain bonds making the material extremely strong and stiff with a tensile strength 3.6 GPa and modulus of ~90 GPa,[30] comparable to the properties of CNT fibers.[31,32] Despite the fact that Kevlar processing might have involved the polymer in the nanoscale state, Kevlar fibers were never associated with nanoscale building blocks of composites. The formation of nanoscale versions of aramid fibers was never experimentally observed or theoretically predicted before.

Instead of the traditional synthesis from monomers used in many other methods of preparation of nanofibers,[3-7] which can also be described as the bottom-to-top approach analogous to the terminology used in many nanoelectronic devices, alternative approaches must be explored for making polymeric structures that would satisfy the needs of both hybrid composites from INCs and multifunctional organic coatings. Importantly, the strength of polymeric components can come not only from the strength of individual polymeric chains but also from their assemblies, which, in turn, underscores the significance of the preparation method. Distribution of stress over multiple polymeric chains allows one to avoid stress concentration at particular bonds, which is the most daunting problem of molecular design of new ultrastrong polymers. Taking this further, we decided to use the so called top-down approach reminiscent to that being used for cellulose[18-26] to prepare suitable polymeric components from macroscale fibers of synthetic polymers, which are known to have high mechanical strength but are processed in a form incompatible with INCs or other polymers.

1. Synthesis of ANFs

Inspired by Takayanagito's work on deprotonation of amide groups,[33,34] Burch *et al.* made aramid films by casting the PPTA solution followed by water immersion[35] or thermal decomposition.[36] In all these studies, the nature of the solution was not studied and it was assumed that the solution consisted of polyanions, which was probably only partially correct. Analyzing these works we realized that fine control over the deprotonation and dissolution process can lead to nanoscale fibers because the balance between electrostatic repulsion and attraction due to π-π and van der Waals interactions must lead to nanoscale version of this material. Notably in many ways the balance of forces and the process itself would be similar to the methods of preparation of graphite dispersions with intermediate step of charged graphene oxide. One could expect that the nanometer-scale forms of Kevlar fibers would possess equally high or better strength, stiffness, toughness and possibly other properties. Nanoscale fibers will allow the distribution of stress over many polymer chains and multiple bonds. This will avoid fast breakage of the weakest bond(s) taking place in non-assembled polymer chains.

High temperatures are known to induce the depolymerization of Kevlar,[35] so we decided to employ a different method of Kevlar dissolution than those used before, which allows for processing to be done at room temperature with minimal reduction of the molecular weight of aramid chains. It was found that the dissolution of Kevlar threads or fabric in KOH splits the bulk macroscale fibers into nanoscale fibers (Figure 1). This process is likely to occur by abstraction of mobile hydrogen from >NH groups and substantial reduction of the strength of hydrogen bonds between the polymer chains (Figures 1f,m), while increasing electrostatic repulsion. Importantly, the extent of this destruction is limited and does not appear to proceed down to the level of individual polymer chains. Complete disintegration of the fibers into individual chains is counteracted by hydrophobic attraction and π-π stacking in the polymer backbone. The diameters of ANFs after the dissolution of Kevlar fabric are 20-30 nm (Figure 1a,g). These diameters decrease with the addition of greater amounts of water (Figure 1b-1d, 1h-1j), reaching 5-10 nm when the volume ratio of water to DMSO is 1:40 (Figure 1d,j). From the materials perspective this is quite remarkable and very convenient for processing into composites although will require further studies. The length of these fibers appears to be in the range of 5 to 10 μm (Figure 1l). ANFs are thicker than single-walled CNTs, which are typically about 1 nm in diameter and several micrometers in length. ANFs are thinner and longer than the cellulose fibers, which are 5-15 nm in diameters and 200 nm to several micrometers in length.[37] Abundance of polar functional groups on ANFs provides additional opportunities compared with CNTs to dramatically improve nanofiber-matrix stress transfer. Note that other potential nanofibers investigated so

far, such as cellulose nanofibers, are quite rigid.[38-42] While materials from them have remarkable properties,[38-42] their successful utilization with INCs, for instance CNTs, to obtain effective stress transfer is impeded by insufficient flexibility as indicated by multiple recent studies.[43-46] Their sensitivity to humidity could also be problematic.[42]

2. ANF Multilayer Assembly

The availability of dispersions makes it possible to utilize a variety of different materials design techniques based on simple liquid processing.[47-51] The layer-by-layer (LBL) assembly technique is one of the most versatile methods for the preparation of organic-inorganic composites with enhanced mechanical parameters.[52] Among other methods of composite synthesis, LBL is advantageous due to intrinsically strong interactions between the components and great uniformity of the resulting materials. Successful examples of LBL composites with exceptional mechanical properties include several INCs.[53,54] It is essential to demonstrate that ANFs can be assembled in LBL systems. It was found that the ANF fibers were both dispersed and ionized in polar solutions and are therefore likely to be suitable for LBL processing. LBL assembly of ANFs was accomplished by using a traditional LBL dipping however only the first layer was PDDA and therefore will be denoted as PDDA/ANF$_n$ where n is the number of dipping cycles in ANF dispersion. The ANFs are fairly uniformly packed on the surface of glass slide during LBL assembly (Figure 2c,d). The gradual growth of ANF multilayers was monitored by ellipsometry and UV-Vis absorption spectra. The growth of PDDA/ANF$_n$ multilayers is nearly linear with the first 10 layers reaching a film thickness of about 16 nm (Figure 2a). This gives a thickness increment for each LBL bilayer of 1.6 nm, which corresponds to fairly loose two-dimensional packing of ANF in each adsorption cycle, as can be seen in the AFM image of Figure 1l.

As more LBL cycles were applied, the enhancement of an absorption peak at around 330 nm, which is characteristic of Kevlar, was observed in the UV-Vis spectrum (Figure 2b). Note that although the initial adsorption of negatively charged ANFs on positively charged PDDA can be attributed to electrostatic interactions, intermediate rinsing with water is expected to regenerate the H^+ on the aramid macromolecules removed by KOH (Figure 1f) and near-electroneutrality of the ANFs. At this moment, stability of ANF films outside of KOH is attributed primarily to aromatic stacking interactions and hydrogen bonding between the multilayer components (Figure 1m), which are also believed to be the main interactions between individual nanofibers. Van der Waals interactions are also expected to contribute to the mechanical integrity of the fibrous network. The successful reconstruction of aramid films with the inclusion of ANFs during the LBL process can be confirmed by Raman scattering (Figure 3a). The Raman spectra of the original macroscale Kevlar material are similar to the results reported before[55], but they are drastically changed after the dissolution in KOH DMSO solution (Figure 3a, see Supporting Information Table S1 for band assignment). These changes disappear after the construction of the ANF films and the Raman spectra of our final films are nearly the same as those of the original Kevlar fibers (Figure 3a). Identification of molecular structures of ANFs in the film was also confirmed by IR spectra (Figure 3c). Compared with Kevlar macrofiber[56], the intensity and sharpness of IR peaks (for example, N-H stretching vibrations) is decreased due to broader distribution of bond lengths and surface states of the fibers. XRD measurements also show broadening of characteristic Kevlar peaks (Figure 3b), which can be assigned to (110), (200) and (004) reflections, respectively[57]. Based on the Scherrer equation, $D = 0.9\lambda/\beta\cos\theta$, where D is the size of crystallites, λ is the wavelength of X-ray beam used in diffraction experiments, β is the line broadening at half the maximum intensity, θ is the Bragg angle, the diameter of the nanofiber can be calculated to be ca. 4.3 nm based on the broadening of (200) reflection obtained after Gaussian peak fitting. This size of crystalline domains matches really well

with the diameter of ANF from TEM observations (Figure 1e), and indicates that the nanoscale fibers retain substantial crystallinity despite reduction in diameter. This fact is also indicative of the retained mechanical properties characteristic of macroscale Kevlar fibers.

3. Physical Properties

The ANF LBL films are transparent allowing for potential use in ultrastrong surface coatings (Figure 4a). They can also be easily peeled from a surface by HF etching[58] (Figure 4c inset). SEM images indicated that a PDDA/ANF_{300} film has a thickness of about 580 nm (Figure 4b), which is comparable to the results of ellipsometry measurements (Figure 2a) and suggests that the average ANF layer is about 1.9 nm thick. Thermogravimetric analysis (TGA) of PDDA/ANF_{300} (Figure 4c) is similar to the bulk Kevlar material.[28] This is very encouraging because heat-resistant, flexible, transparent films represent a bottleneck for many applications in flexible electronics and flexible photovoltaic cells based on semiconductors with high electron/hole mobility.[59]

It is expected that PDDA/ANF_n films will be elastically orthotropic, with the in-plane and out-of-plane properties being different as is the case with clay and many other multilayers.[60,61] Brillouin light scattering (BLS) is a convenient method to determine the orthotropic moduli.[62,63] The in-plane and out-of-plane longitudinal moduli were determined to be 22 ± 1.2 GPa and 11.8 ± 0.6 GPa, respectively (Figure 4d, Table 1). A higher in-plane modulus is expected as ANFs are spread on the substrate with axes parallel to the plane. PDDA/ANF_n films outperform a well-known high-performance polymeric coating material, *i.e*., polyimide thin film with 17.7 GPa in-plane longitudinal modulus and 7.7 GPa out-of-plane longitudinal modulus recently probed by a similar technique.[63] These mechanical properties of PDDA/ANF_n films also exceed those for cellulose nanofibers[38-46] with no effect of humidity that greatly reduces the performance of cellulose LBL films.[42] Furthermore, the Young's modulus is 10-20 times higher than that of aligned cellulose fibers and CNTs.[43-46]

The compression stiffness and hardness of the ANF LBL films were estimated using a Berkovich nanoindenter at various indentation depths. Care was taken to ensure that the depths of the indentations were shallow enough to avoid significant influence from the substrate, which was indeed detected at greater penetration depths (Figure 5 and Supporting Information Figure S1). The tests revealed a hardness of 0.46 ± 0.04 GPa (Figure 5c, Table 1) for our film, which is higher than some high strength polymers, such as isotactic polypropylene (H = 0.125 GPa) and high-density polyethylene (H = 0.06 GPa).[64] The Young's modulus was obtained using the continuous stiffness measurement technique of Oliver and Pharr[65] during both the loading and unloading portions of the indentation. The film was found to have a modulus value of 9 ± 1 GPa (Table 1), and the value appeared not to be affected by the substrate for indentation depths of less than 200 nm (Figure 5d). The modulus of the films was higher than the 5.5 GPa reported for a cast film of pure Kevlar.[35] This indicates that the preparation of ANFs is indeed advantageous for preparation of high-performance materials. Solvent-based LBL process is particularly effective at producing reasonably dense and better ordered arrays of the nanofibers, compared with the casting technique. The modulus is also higher than the reported elastic modulus obtained from nanoindentation of various uniaxial anisotropic polyimide films, which were in the range of 5 to 7 GPa.[66,67] Since BLS measures the longitudinal modulus, the corresponding Young's modulus can be extracted,[68] assuming a Poisson's ratio of 0.25,[69] resulting in a value of 9.8 ± 0.5 GPa, which compares remarkably well with the nanoindentation measurement of 9 ± 1 GPa.

Conclusions

Negatively-charged, uniformly-sized ANFs can be prepared in DMSO media by controlled deprotonation with KOH. The diameter of the fibers can be effectively controlled by addition of water. Such dispersions represent the first example of nanofiber dispersions of synthetic polymers. They are suitable for making nanoscale materials using many techniques and can be considered as new nanoscale building blocks for ultrastrong materials. They also reveal intriguing similarities to CNTs in respect to morphology and mechanical behavior in polymer composites. As a potential direction of future research, evaluation of the mechanical properties of individual ANF to compare those to carbon nanotubes would be quite interesting from both fundamental and practical perspectives. We believe that the method demonstrated here provides a way to prepare ANF-based high-performance films and to incorporate ANFs into multifunctional films lending its outstanding mechanical properties to the resulting hybrid material(s).

Experimental Section

Preparation of aramid nanofiber solutions

1 g of bulk Kevlar 69 (from Thread Exchange, right twist) and 1.5 g KOH were added into 500 ml dimethyl sulfoxide (DMSO) which was magnetically stirred for 1 week at room temperature forming a dark red solution of ANFs. For the preparation of ANF films, the microscope glass slides used in LBL assembly were cleaned in piranha solution (3:1 H_2SO_4:H_2O_2) for 24 h, followed by thorough rinsing with deionized water prior to use.

LBL assembly of aramid nanofibers

A clean piece of glass slide was first dipped into 1% poly(diallyldimethylammonium chloride) (PDDA) solution for 1 min and rinsed with water for 2 min before air drying. As the piranha solution treatment leaves the surface of the substrate negatively charged which results in electrostatic repulsion of ANFs with the same charges, the initial layer of PDDA is essential for film growth, without it no Kevlar is observed on the substrate. The PDDA coated glass slide can then be used for the deposition of ANFs. The PDDA coated glass slide was dipped into the Kevlar DMSO solution for 1 minute and rinsed with water for 2 min before air drying and this sequence of steps was repeated 300 times. The film is easily peeled from the substrate by immersing in 1% HF solution.

Instruments and testing

Atomic-force microscopy (AFM) experiments were performed in tapping mode using a NanoScope IIIa (Veeco Instruments, Santa Barbara, CA). The sample for AFM testing was prepared by immersing a PDDA-coated silicon wafer into Kevlar DMSO solution followed by water rinsing and air drying. Transmission-electron microscopy (TEM) characterizations of Kevlar/DMSO diluted aqueous solutions were obatined using a JEOL 3011 high-resolution electron microscope. One drop of the different solutions was placed on the surface of a copper grid coated with carbon and dried in the oven at 110 °C before testing.

For TEM observation of the single bilayer PDDA/ANFs, a TEM grid was coated with PDDA and then with ANFs using an LBL assembly process similar to that used with the glass slides. Scanning-electron microscopy (SEM) images were obtained from a gold-coated film using an FEI Nova NanoLab dual-beam FIB and scanning electron microscope on gold-coated film. The LBL film growth was monitored using an 8453 UV-Vis ChemStation spectrophotometer (Agilent Technologies) with a fresh, piranha-cleaned glass slide used as a reference. Ellipsometry measurements were obtained using a BASE-160 Spectroscopic Ellipsometer (J. A. Woollam Co., Inc.). The samples used for ellipsometry were prepared on

silicon wafers as described previously. Thermogravimetric analysis (TGA) was performed using a Perkin-Elmer DSC-7 (PerkinElmer, Wellesley, MA). Resonance Raman spectra were taken with a Dimension-P1 Raman system (Lambda Solutions, Inc.) with 532 nm excitation. IR spectra were obtained using a Nicolet 6700 spectrometer utilizing the grazing angle accessory (Smart SAGA) at a grazing angle of 85°. X-ray diffraction (XRD) measurement was performed using Rigaku rotating Anode XRD with Cu Kα generated at 40 kV and 100 mA, and a scanning speed of 0.2°/min. The mechanical properties of LBL films were tested using a Nanoinstruments NanoIndenter II model provided by MTS Nanoinstruments Inc., Oak Ridge, TN. A Berkovich-shaped indenter was used, and the hardness and elastic modulus (indentation modulus) were calculated and recorded from five different testing points. The analysis of nanoindentation data was performed using the Oliver and Pharr method, assuming a value of 0.25 for the Poisson's ratio of the film.

Brillouin light scattering (BLS) measurements were performed in backscattering geometry with an incident angle close to the surface normal, as described elsewhere.[70] In this geometry, light that scattered from phonons propagating in the near out-of-plane direction is collected at 180° from the incident beam as shown in Supporting Information Scheme S1. For thin-film samples, the light redirected from a reflective substrate and scattered from phonons propagating in the in-plane direction, akin to the standard platelet geometry, can also be captured by the same collection optics, giving rise to the so-called 2α-peak. This geometry allows for the simultaneous measurement of the in-plane and out-of-plane elastic moduli. Samples were probed using a Coherent Verdi solid-state laser with a wavelength of 532 nm where the laser intensity illuminating the sample was less than 10 mW. The laser light was focused onto the sample with a focusing spot of ~50 μm in diameter and 1 μm in depth. The scattered light was collected over a period of ~30 min, and analyzed using a Sandercock 6 pass tandem Fabry-Perot interferometer. Several measurements were taken at different spots on the film in order to assure reproducibility and film homogeneity. The density of ANFs film was estimated by weighing pieces of rectangular films with known dimensions.

Supplementary Material

Refer to Web version on PubMed Central for supplementary material.

Acknowledgments

The authors would like to express their gratitude to ONR for primary support of this research with a grant #N00014-06-1-0473. Strong support of this work by AFOSR grant GRT00008581/RF60012388 (NAK) is also acknowledged. This material is also based upon work partially supported by the Center for Solar and Thermal Energy Conversion, an Energy Frontier Research Center funded by the U.S. Department of Energy, Office of Science, Office of Basic Energy Sciences under Award Number #DE-SC0000957. We acknowledge support from NSF under grant ECS-0601345; EFRI-BSBA 0938019; CBET 0933384; CBET 0932823; and CBET 1036672. The work is also partially supported by AFOSR MURI 444286-P061716 and NIH 1R21CA121841-01A2. The authors thank the University of Michigan's EMAL for its assistance with electron microscopy, and for the NSF grant #DMR-9871177 for funding for the JEOL 2010F analytical electron microscope used in this work.

References

1. Torquato S. Modeling of Physical Properties of Composite Materials. Int J Solids Struct. 2000; 37:411–422.
2. Torquato S, Hyun S, Donev A. Multifunctional Composites: Optimizing Microstructures for Simultaneous Transport of Heat and Electricity. Phys Rev Lett. 2002; 89:266601. [PubMed: 12484843]
3. Greiner A, Wendorff JH. Electrospinning: A Fascinating Method for the Preparation of Ultrathin Fibres. Angew Chem -Int Edit Engl. 2007; 46:5670–5703.

4. Ondarcuhu T, Joachim C. Drawing a Single Nanofibre Over Hundreds of Microns. Europhys Lett. 1998; 42:215–220.
5. Feng L, Li SH, Li HJ, Zhai J, Song YL, Jiang L, Zhu DB. Super-Hydrophobic Surface of Aligned Polyacrylonitrile Nanofibers. Angew Chem -Int Edit Engl. 2002; 41:1221–1223.
6. Zhang RY, Ma PX. Poly(alpha-hydroxyl acids) Hydroxyapatite Porous Composites for Bone-Tissue Engineering. I. Preparation and Morphology. J Biomed Mater Res. 1999; 44:446–455. [PubMed: 10397949]
7. Hartgerink JD, Beniash E, Stupp SI. Self-Assembly and Mineralization of Peptide-Amphiphile Nanofibers. Science. 2001; 294:1684–1688. [PubMed: 11721046]
8. Martin CR. Nanomaterials - A Membrane-Based Synthetic Approach. Science. 1994; 266:1961–1966. [PubMed: 17836514]
9. Martin CR. Template Synthesis of Electronically Conductive Polymer Nanostructures. Accounts Chem Res. 1995; 28:61–68.
10. Park S, Lim JH, Chung SW, Mirkin CA. Self-Assembly of Mesoscopic Metal-Polymer Amphiphiles. Science. 2004; 303:348–351. [PubMed: 14726585]
11. Hurst SJ, Payne EK, Qin LD, Mirkin CA. Multisegmented One-Dimensional Nanorods Prepared by Hard-Template Synthetic Methods. Angew Chem -Int Edit Engl. 2006; 45:2672–2692.
12. Huang LM, Wang ZB, Wang HT, Cheng XL, Mitra A, Yan YS. Polyaniline Nanowires by Electropolymerization from Liquid Crystalline Phases. J Mater Chem. 2002; 12:388–391.
13. Huang JX, Kaner RB. A General Chemical Route to Polyaniline Nanofibers. J Am Chem Soc. 2004; 126:851–855. [PubMed: 14733560]
14. Huang JX, Virji S, Weiller BH, Kaner RB. Polyaniline Nanofibers: Facile Synthesis and Chemical Sensors. J Am Chem Soc. 2003; 125:314–315. [PubMed: 12517126]
15. Tang ZY, Kotov NA, Giersig M. Spontaneous Organization of Single CdTe Nanoparticles into Luminescent Nanowires. Science. 2002; 297:237–240. [PubMed: 12114622]
16. Sone ED, Zubarev ER, Stupp SI. Semiconductor Nanohelices Templated by Supramolecular Ribbons. Angew Chem -Int Edit Engl. 2002; 41:1705–1709.
17. Zhang SM, Greenfield MA, Mata A, Palmer LC, Bitton R, Mantei JR, Aparicio C, de la Cruz MO, Stupp SI. A Self-Assembly Pathway to Aligned Monodomain Gels. Nat Mater. 2010; 9:594–601. [PubMed: 20543836]
18. Eichhorn SJ, Dufresne A, Aranguren M, Marcovich NE, Capadona JR, Rowan SJ, Weder C, Thielemans W, Roman M, Renneckar S, et al. Review: Current International Research into Cellulose Nanofibres and Nanocomposites. J Mater Sci. 2010; 45:1–33.
19. Nogi M, Iwamoto S, Nakagaito AN, Yano H. Optically Transparent Nanofiber Paper. Adv Mater. 2009; 21:1595–1598.
20. Sarrazin P, Valecce L, Beneventi D, Chaussy D, Vurth L, Stephan O. Photoluminescent Paper Based on Poly(fluorene-co-fluorenone) Particles Adsorption on Modified Cellulose Fibers. Adv Mater. 2007; 19:3291–3294.
21. Capadona JR, Shanmuganathan K, Tyler DJ, Rowan SJ, Weder C. Stimuli-Responsive Polymer Nanocomposites Inspired by the Sea Cucumber Dermis. Science. 2008; 319:1370–1374. [PubMed: 18323449]
22. Fukuzumi H, Saito T, Wata T, Kumamoto Y, Isogai A. Transparent and High Gas Barrier Films of Cellulose Nanofibers Prepared by TEMPO-Mediated Oxidation. Biomacromolecules. 2009; 10:162–165. [PubMed: 19055320]
23. Elazzouzi-Hafraoui S, Nishiyama Y, Putaux JL, Heux L, Dubreuil F, Rochas C. The Shape and Size Distribution of Crystalline Nanoparticles Prepared by Acid Hydrolysis of Native Cellulose. Biomacromolecules. 2008; 9:57–65. [PubMed: 18052127]
24. Hubbe MA, Rojas OJ, Lucia LA, Sain M. Cellulosic Nanocomposites: A Review. BioResources. 2008; 3:929–980.
25. Saito T, Kimura S, Nishiyama Y, Isogai A. Cellulose Nanofibers Prepared by TEMPO-Mediated Oxidation of Native Cellulose. Biomacromolecules. 2007; 8:2485–2491. [PubMed: 17630692]
26. Eichhorn SJ. Cellulose Nanowhiskers: Promising Materials for Advanced Applications. Soft Matter. 2011; 7:303–315.

27. Podsiadlo P, Tang ZY, Shim BS, Kotov NA. Counterintuitive Effect of Molecular Strength and Role of Molecular Rigidity on Mechanical Properties of Layer-by-Layer Assembled Nanocomposites. Nano Lett. 2007; 7:1224–1231. [PubMed: 17455982]
28. Tanner D, Fitzgerald JA, Phillips BR. The Kevlar Story - An Advanced Materials Case-Study. Angew Chem -Int Edit Engl. 1989; 28:649–654.
29. Chae HG, Kumar S. Rigid-Rod Polymeric Fibers. J Appl Polym Sci. 2006; 100:791–802.
30. Vollrath F, Knight DP. Liquid Crystalline Spinning of Spider Silk. Nature. 2001; 410:541–548. [PubMed: 11279484]
31. Koziol K, Vilatela J, Moisala A, Motta M, Cunniff P, Sennett M, Windle A. High-Performance Carbon Nanotube Fiber. Science. 2007; 318:1892–1895. [PubMed: 18006708]
32. O'Connor I, Hayden H, O'Connor S, Coleman JN, Gun'ko YK. Kevlar Coated Carbon Nanotubes for Reinforcement of Polyvinylchloride. J Mater Chem. 2008; 18:5585–5588.
33. Takayanagi M, Katayose T. N-Substituted Poly(p-phenylene terephthalamide). J Polym Sci Pol Chem. 1981; 19:1133–1145.
34. Takayanagi M, Kajiyama T, Katayose T. Surface-Modified Kevlar Fiber-Reinforced Polyethylene and Ionomer. J Appl Polym Sci. 1982; 27:3903–3917.
35. Burch RR, Sweeny W, Schmidt HW, Kim YH. Preparation of Aromatic Polyamide Polyanions – A Novel Processing Strategy for Aromatic Polyamides. Macromolecules. 1990; 23:1065–1072.
36. Burch RR, Manring LE. N-Alkylation and Hofmann Elimination from Thermal-Decomposition of R_4N^+ Salts of Aromatic Polyamide Polyanions – Synthesis and Stereochemistry of N-Alkylated Aromatic Polyamides. Macromolecules. 1991; 24:1731–1735.
37. Podsiadlo P, Choi SY, Shim B, Lee J, Cuddihy M, Kotov NA. Molecularly Engineered Nanocomposites: Layer-by-Layer Assembly of Cellulose Nanocrystals. Biomacromolecules. 2005; 6:2914–2918. [PubMed: 16283706]
38. Berglund LA, Peijs T. Cellulose Biocomposites-From Bulk Moldings to Nanostructured Systems. MRS Bull. 2010; 35:201–207.
39. Isogai A, Saito T, Fukuzumi H. TEMPO-Oxidized Cellulose Nanofibers. Nanoscale. 2011; 3:71–85. [PubMed: 20957280]
40. Siro I, Plackett D. Microfibrillated Cellulose and New Nanocomposite Materials: A Review. Cellulose. 2010; 17:459–494.
41. Shanmuganathan K, Capadona JR, Rowan SJ, Weder C. Biomimetic Mechanically Adaptive Nanocomposites. Prog Polym Sci. 2010; 35:212–222.
42. Cranston ED, Eita M, Johansson E, Netrval J, Salajkova M, Arwin H, Wagberg L. Determination of Young's Modulus for Nanofibrillated Cellulose Multilayer Thin Films Using Buckling Mechanics. Biomacromolecules. 2011; 12:961–969. [PubMed: 21395236]
43. Chen P, Yun YS, Bak H, Cho SY, Jin HJ. Multiwalled Carbon Nanotubes-Embedded Electrospun Bacterial Cellulose Nanofibers. Mol Cryst Liq Cryst. 2010; 519:169–178.
44. Li M, Kim IH, Jeong YG. Cellulose Acetate/Multiwalled Carbon Nanotube Nanocomposites with Improved Mechanical, Thermal, and Electrical Properties. J Appl Polym Sci. 2010; 118:2475–2481.
45. Miyauchi M, Miao J, Simmons TJ, Lee JW, Doherty TV, Dordick JS, Linhardt RJ. Conductive Cable Fibers with Insulating Surface Prepared by Coaxial Electrospinning of Multiwalled Nanotubes and Cellulose. Biomacromolecules. 2010; 11:2440–2445. [PubMed: 20690644]
46. Lu P, Hsieh YL. Multiwalled Carbon Nanotube (MWCNT) Reinforced Cellulose Fibers by Electrospinning. ACS Appl Mater Interfaces. 2010; 2:2413–2420. [PubMed: 20669908]
47. Park S, Lee KS, Bozoklu G, Cai W, Nguyen ST, Ruoff RS. Graphene Oxide Papers Modified by Divalent Ions - Enhancing Mechanical Properties *via* Chemical Cross-Linking. ACS Nano. 2008; 2:572–578. [PubMed: 19206584]
48. Walther A, Bjurhager I, Malho JM, Pere J, Ruokolainen J, Berglund LA, Ikkala O. Large-Area, Lightweight and Thick Biomimetic Composites with Superior Material Properties *via* Fast, Economic, and Green Pathways. Nano Lett. 2010; 10:2742–2748. [PubMed: 20218653]
49. Hu L, Hecht DS, Gruner G. Percolation in Transparent and Conducting Carbon Nanotube Networks. Nano Lett. 2004; 4:2513–2517.

50. Dikin DA, Stankovich S, Zimney EJ, Piner RD, Dommett GHB, Evmenenko G, Nguyen ST, Ruoff RS. Preparation and Characterization of Graphene Oxide Paper. Nature. 2007; 448:457–460. [PubMed: 17653188]
51. Wu ZC, Chen ZH, Du X, Logan JM, Sippel J, Nikolou M, Kamaras K, Reynolds JR, Tanner DB, Hebard AF, Rinzler AG. Transparent, Conductive Carbon Nanotube Films. Science. 2004; 305:1273–1276. [PubMed: 15333836]
52. Decher G. Fuzzy Nanoassemblies: Toward Layered Polymeric Multicomposites. Science. 1997; 277:1232–1237.
53. Podsiadlo P, Kaushik AK, Arruda EM, Waas AM, Shim BS, Xu JD, Nandivada H, Pumplin BG, Lahann J, Ramamoorthy A, Kotov NA. Ultrastrong and Stiff Layered Polymer Nanocomposites. Science. 2007; 318:80–83. [PubMed: 17916728]
54. Tang ZY, Kotov NA, Magonov S, Ozturk B. Nanostructured Artificial Nacre. Nat Mater. 2003; 2:413–418. [PubMed: 12764359]
55. Washer G, Brooks T, Saulsberry R. Investigating the Effects of Aging on the Raman Scattering of Kevlar Strands. Res Nondestruct Eval. 2008; 19:144–163.
56. Crompton, TR. Polymer Reference Book. Smithers Rapra Technology; 2006. p. 181-182.
57. Jain A, Vijayan K. Kevlar 49 Fibres: Thermal Expansion Coefficients from High Temperature X-Ray Data. Curr Sci. 2000; 78:331–335.
58. Mamedov AA, Kotov NA, Prato M, Guldi DM, Wicksted JP, Hirsch A. Molecular Design of Strong Single-Wall Carbon Nanotube/Polyelectrolyte Multilayer Composites. Nat Mater. 2002; 1:190–194. [PubMed: 12618809]
59. Nomura K, Ohta H, Takagi A, Kamiya T, Hirano M, Hosono H. Room-Temperature Fabrication of Transparent Flexible Thin-Film Transistors Using Amorphous Oxide Semiconductors. Nature. 2004; 432:488–492. [PubMed: 15565150]
60. Kumar SR, Renusch DP, Grimsditch M. Effect of Molecular Orientation on the Elastic Constants of Polypropylene. Macromolecules. 2000; 33:1819–1826.
61. Kurabayashi K, Goodson KE. Impact of Molecular Orientation on Thermal Conduction in Spin-Coated Polyimide Films. J Appl Phys. 1999; 86:1925–1931.
62. Nizzoli F, Hillebrands B, Lee S, Stegeman GI, Duda G, Wegner G, Knoll W. Determination of the Whole Set of Elastic-Constants of a Polymeric Langmuir-Blodgett Film by Brillouin Spectroscopy. Phys Rev B. 1989; 40:3323–3328.
63. Gomopoulos N, Saini G, Efremov M, Nealey PF, Nelson K, Fytas G. Nondestructive Probing of Mechanical Anisotropy in Polyimide Films on Nanoscale. Macromolecules. 2010; 43:1551–1555.
64. Podsiadlo P, Michel M, Lee J, Verploegen E, Kam NWS, Ball V, Qi Y, Hart AJ, Hammond PT, Kotov NA. Exponential Growth of LBL Films with Incorporated Inorganic Sheets. Nano Lett. 2008; 8:1762–1770. [PubMed: 18484777]
65. Oliver WC, Pharr GM. Measurement of Hardness and Elastic Modulus by Instrumented Indentation: Advances in Understanding and Refinements to Methodology. J Mater Res. 2004; 19:3–20.
66. Lee C, Kwon J, Park S, Sundar S, Min B, Han H. Nanoindentation Studies of Polyimide Thin Films with Various Internal Linkages in the Diamine Component. J Polym Sci Pt B Polym Phys. 2004; 42:861–870.
67. Jang W, Seo J, Lee C, Paek SH, Han H. Residual Stress and Mechanical Properties of Polyimide Thin Films. J Appl Polym Sci. 2009; 113:976–983.
68. The longitudinal modulus, C_{11}, is related to the Young's modulus, E, and Poisson's ratio, ν, through the formula, $C_{11}=E(1-\nu)/(1+\nu)(1-2\nu)$.
69. Nakamae K, Nishino T, Xu AR. Poissons Ratio of the Crystal-Lattice of Poly(p-phenylene terephthalamide) by X-Ray-Diffraction. Polymer. 1992; 33:4898–4900.
70. Sui L, Huang L, Podsiadlo P, Kotov NA, Kieffer J. Brillouin Light Scattering Investigation of the Mechanical Properties of Layer-by-Layer Assembled Cellulose Nanocrystal Films. Macromolecules. 2010; 43:9541–9548.

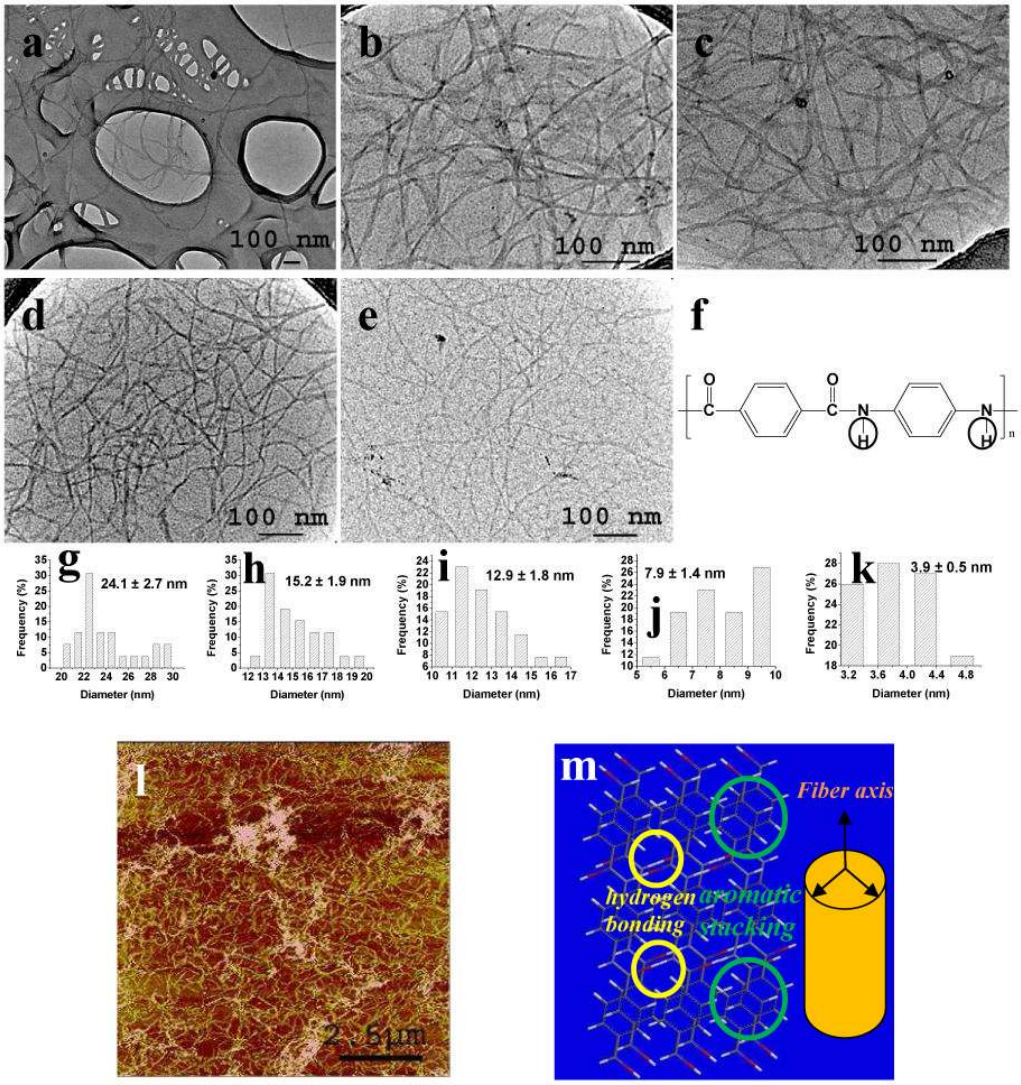

Figure 1.

TEM images of ANFs in DMSO solution with different water to DMSO volume ratios: a) 0, b) 1/200, c) 1/100 and d) 1/40. e) TEM image of one bilayer PDDA/ANFs. f) The molecular structure of aramid; the H atoms removed by KOH are marked by circles. (g-k) Statistical analysis of diameter distribution for ANFs under same conditions as that shown in a-e, respectively. l) AFM image of one bilayer PDDA/ANFs. m) Molecular description of ANFs. Yellow circles mark the inter-molecular hydrogen bonds formed between the carbonyl groups and >NH groups; green circles mark aromatic stacking interactions between adjacent strands. The approximate length range of ANFs was estimated to be 5-10 μm, based on Figure 1l.

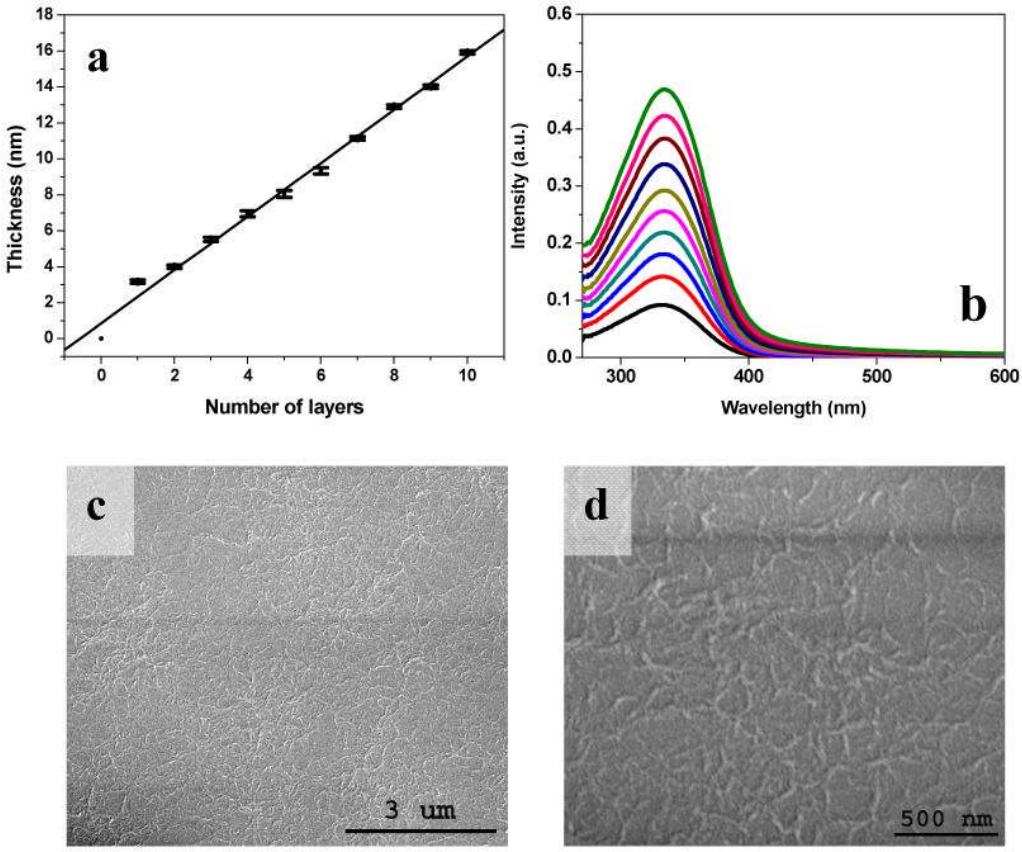

Figure 2.

a) Ellipsometry results for LBL assembly of ANFs on silicon substrate. b) UV-Vis spectra of 1-10 layers of ANF films (from bottom to top: 1-10 layers of ANFs). c and d are SEM images of one bilayer PDDA/ANFs on a glass slide.

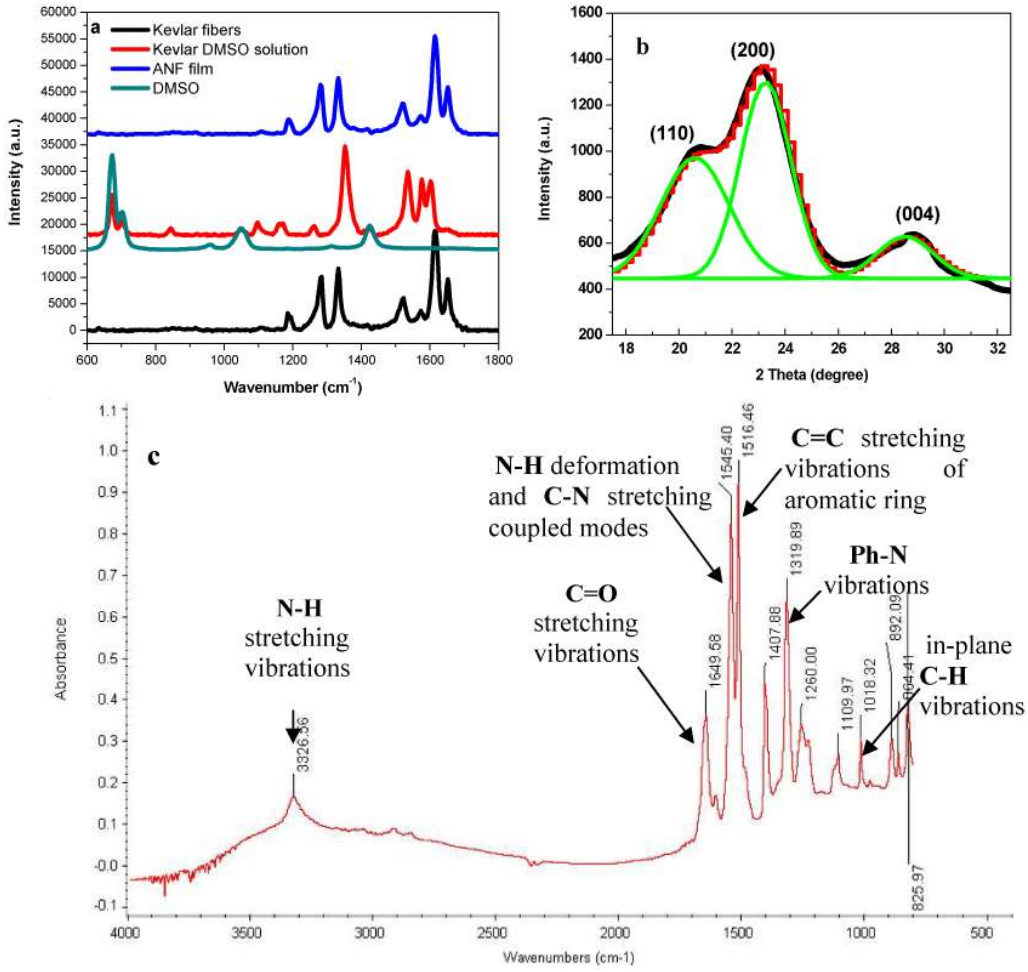

Figure 3.

a) Raman scattering of Kevlar fibers (black line), Kevlar DMSO solution (red line) and ANF film (blue line). The Raman scattering of DMSO (green line) is also given near the spectra of Kevlar DMSO solution to clarify the solvent influence. b) XRD pattern of ANF film (black line) with Gaussian peak fitting (green and red lines). c) IR spectra of ANF film with main peaks assignment.

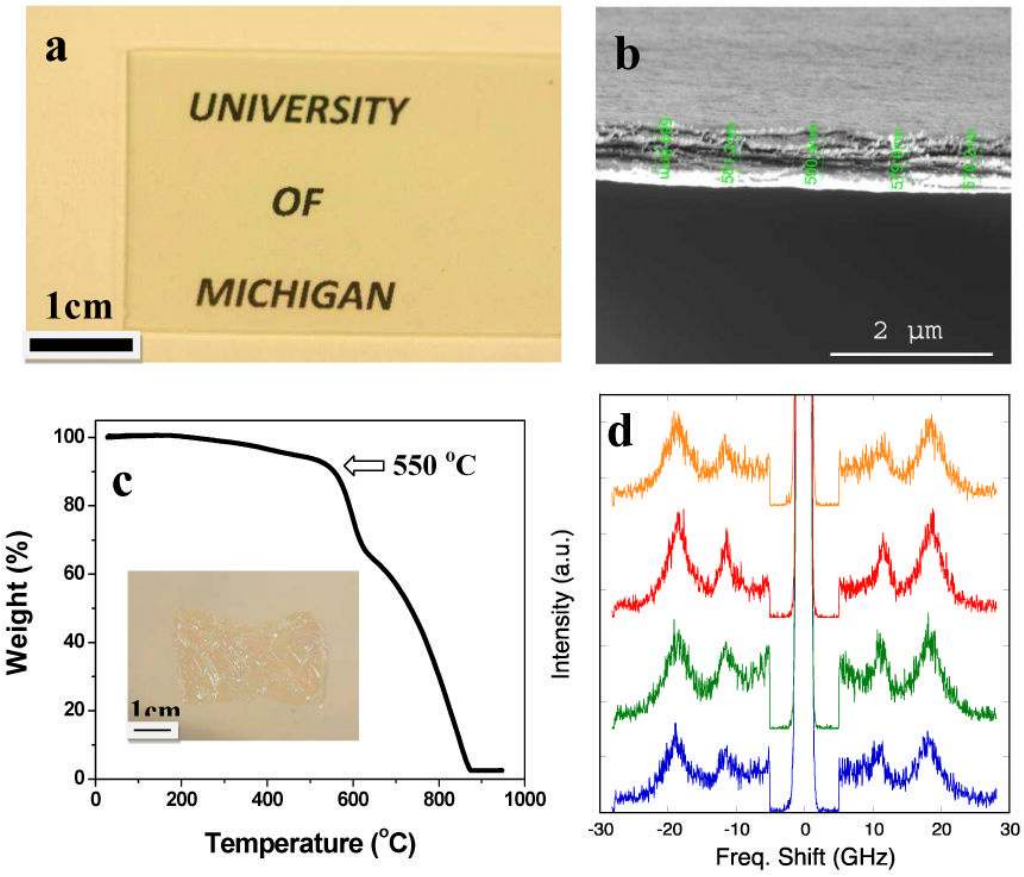

Figure 4.

a) Optical image of 300 layers LBL ANF film on glass slide, b) cross-sectional SEM image of PDDA/ANF_{300} and c) thermogravimetric analysis of PDDA/ANF_{300}. Inset: free-standing PDDA/ANF_{300} film. d) Stokes and anti-Stokes peak of the Brillouin Spectra for PDDA/ANF_{300} taken at four different spots, the spectra are offset for the ease of viewing.

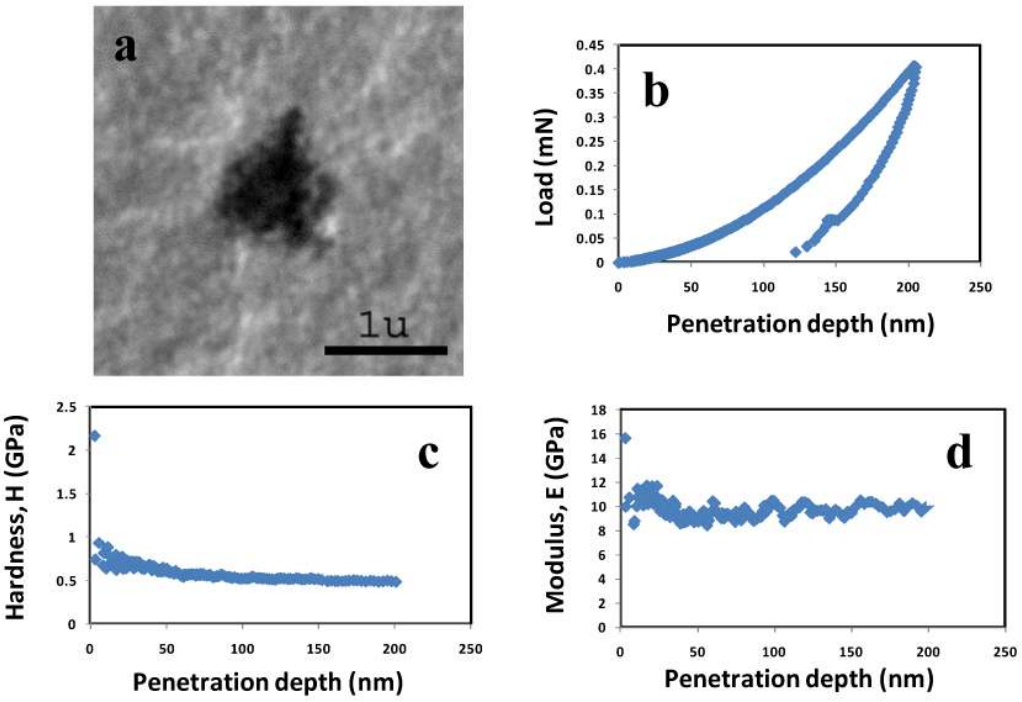

Figure 5.

Typical results from nanoindentation experiments for PDDA/ANF_{300} LBL film with maximum depth set at 200 nm. a) SEM images of an indent left by a Berkovich tip in PDDA/ANF_{300} film. b) Represents load-displacement curve. c) Represents the hardness as a function of penetration depth and d) corresponding modulus. These results are from the loading part of the experiment.

Table 1

A) Summary of modulus and hardness derived from loading and unloading part. B) Summary of in-plane and out-of-plane modulus obtained from Brillouin light scattering.

A-nanoindentation	**Loading**	**Unloading**
Modulus (GPa)	9 ± 1	8 ± 1
Hardness (GPa)	0.46 ± 0.04	0.45 ± 0.05
B-Brillouin light scattering	In plane	Out of plane
Modulus (GPa)	22 ± 1.1	11.8 ± 0.6